Quantification of the 3-D Electromagnetic Power Absorption Rate in Tissue During Transurethral Prostatic Microwave Thermotherapy Using Heat Transfer Model

Liang Zhu, Lisa X. Xu,* and Norbert Chencinski

***Abstract*—Experiments were performed in a tissue microwave-equivalent phantom gel to quantitatively examine the volumetric heating produced by a microwave antenna with a peripheral cooling system for the transurethral prostatic thermotherapy. Based on previous research, expression for the specific absorption rate (SAR) of microwave energy in the gel was extended to three dimensions, which includes its dependence on radial, angular, and axial direction. A theoretical heat transfer model was developed to study the temperature distribution in the gel by introducing this proposed SAR expression. The parameters in this expression and the convection coefficient due to the chilled water running around the antenna were determined using a least-square residual fit of the theoretical temperature predictions to the experimentally measured steady-state temperature field within the gel. The analytical expression of the three-dimensional SAR distribution obtained in this study will help provide a better understanding of the microwave heating pattern in the prostatic tissue and, thus, to aid in designing improved applicators. It can also be used in the future as an accurate input to heat transfer models which predict temperature distributions during the transurethral microwave thermotherapy.**

***Index Terms*— Heat transfer model, microwave heating, prostate, specific absorption rate (SAR), thermotherapy.**

NOMENCLATURE

A_t	Constant in SAR expression.
B	Magnitude of the electromagnetic field.
C_t	Constant in (4).
h	Convective coefficient (W/m^2/K).
k	Thermal conductivity of the gel (W/m/K).
q'''	Volumetric heat rate (W/mm^3).
Q	Microwave power level (W).
r	Radial distance (mm).
r_i	Inner radius of the gel (mm).
r_0	Outer radius of the gel (mm).
R	Coefficient of determination for least-square fitted curve.
s	Offset of the antenna from the geometric center of the catheter (mm).
SAR	Specific absorption rate (W/mm^3).
T	Gel temperature.
T_w	Cooling water temperature (°C).
T_∞	Environment temperature (°C).
W	Green's function.
x, y	Cartesian coordinate.
z	Axial distance (mm).
z_0	Axial decay distance in (4) (mm).
α	Attenuation constant (mm^{-1}).
Δ	Temperature difference $= T - T'$ (°C).
θ	Angle.
ξ, η, λ	Cylindrical coordinates of the source point.

Manuscript received February 7, 1997; revised April 30, 1998. This work was supported by the National Institutes of Health (NIH) under Grant 5 R29CA67970-01. *Asterisk indicates corresponding author.*

L. Zhu was with the Department of Applied Sciences, College of Staten Island of the City University of New York, Staten Island, NY 10314 USA. She is now with the Department of Mechanical Engineering, University of Maryland at Baltimore County, Baltimore, MD 21250 USA.

*L. Xu was with the Department of Applied Sciences, College of Staten Island of the City University of New York, Staten Island, NY 10314 USA. She is now with the School of Mechanical Engineering, 1288 Engineering Building, Purdue University, West Lafayette, IN 47907 USA (e-mail: lxu@ecn.purdue.edu).

N. Chencinski is with the Department of Applied Sciences, College of Staten Island of the City University of New York, Staten Island, NY 10314 USA.

Publisher Item Identifier S 0018-9294(98)06091-1.

I. INTRODUCTION

LOCALIZED microwave thermal therapy has been proposed as one of the nonsurgical modalities for treatment of symptomatic benign prostatic hyperplasia (BPH) [2], [3], [7], [11], [13], [16], [18], [20], [22], [23]. Currently, the hyperthermia system using a symmetrically radiating applicator located within the prostatic urethra has attracted a great deal of attention. To produce more effective symptomatic relief of BPH, it is the clinical intent to heat and cause coagulation necrosis in target tissue within the prostate while simultaneously preserving the surrounding healthy tissue, especially the urethra.

The goal of microwave treatment in the BPH patient is permanent thermoablation of the obstructive prostate tissue without significant injury to adjacent tissues. The likelihood of treatment success is related to the administration of an optimal thermal dose, that is, exposure to a sufficiently elevated temperature for a sufficiently prolonged time period to thermoablate the target tissue. To improve treatment efficacy, any increase in the thermal dose can only be achieved through a better understanding and more accurate predictions on the tissue temperature rise resulted from both the natural (blood flow) and man-imposed (thermal dose and microwave heating pattern) thermoregulation processes. Thus, to accurately model

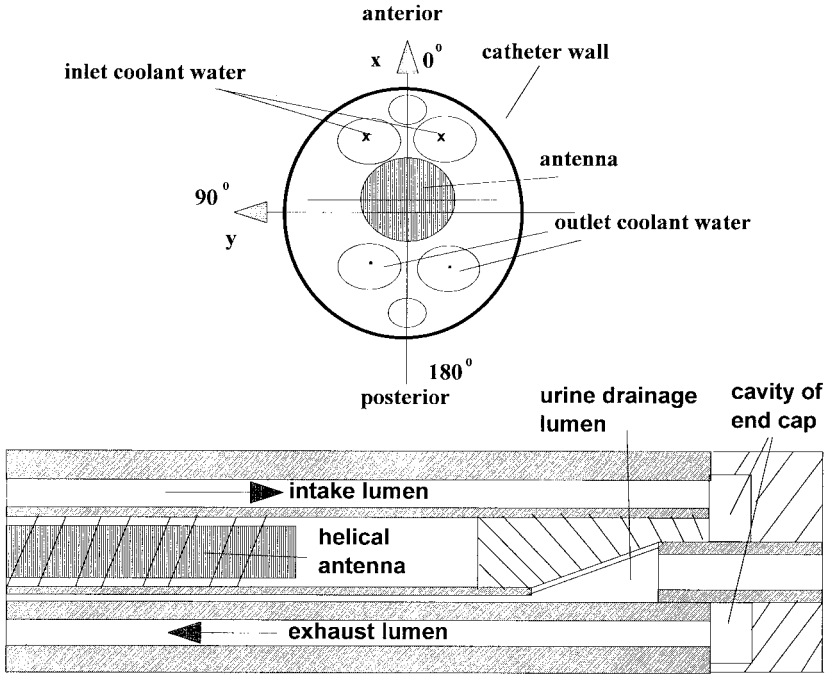

Fig. 1. Schematic of the cross-sectional and the sectional view of the proximal end of the T3 catheter.

the thermal field during the transurethral therapy, the volumetric heating in the prostate induced by the T3 system, namely, the specific absorption rate (SAR), must be first investigated [17].

There are a number of previous investigations of the SAR distributions for various microwave antennas [4]–[6], [9], [10], [17], [19], [24], [25], which provided important information in improving the microwave antenna. For example, the measurements of SAR showed that the heating pattern outside the helical antenna had better longitudinal homogeneity than the coaxial dipole antenna and avoided the hot spot associated with the dipole junction. Several approaches were used to determine the SAR distribution. It can be derived based on the Maxwell equation of the electromagnetic (EM) field [10]. This method usually involves numerical calculation and is relatively difficult to use. In most investigations, the SAR values at various locations were measured by determining the initial rate of temperature rise immediately following a step increase in the applied power [4]–[6], [10], [17], [25]–[27]. This method is highly approximated if heat conduction can be negligible at the instant of microwave power on. A curve fitting is used to obtain an expression for the SAR distribution. To obtain an accurate expression for SAR distribution enough temperature sensors should be placed in the region where the microwave energy is absorbed. However, the SAR decays rapidly in the radial direction due to the superficial penetration of the energy and it is difficult to place many temperature sensors in the near field, which can affect the accuracy of the SAR expression.

The transurethral thermal therapy (T3) system is designed to deliver controlled microwave energy to target areas within the prostate (bilaterally in the transition zones) transurethrally via a Foley-type catheter, which includes a cooling system to prevent thermal damage to the prostatic urethra (Fig. 1). The microwave antenna is a helical antenna. Inside the catheter, there is a coaxial cable, the terminal end of which has a flat wire element wound about an outer insulator of the coaxial cable. An intermediate point of the helical element is electrically connected to an outer conductor of the coaxial cable, thereby dividing the helical element into first and second sections having opposing poles. A series capacitance is connected between an inner conductor of the coaxial cable and a point on the second helical element where the resistive component of the antenna's impedance matches the characteristic impedance of the coaxial cable. The helical element forming the antenna has an effective electrical length which is generally equal to one half the wavelength of the radiation emitted in the surrounding medium, independent of the physical length of the element. There are two intake lumens from the distal shaft end to its proximal end of the catheter where the intake lumens are exposed to cavity of the end cap of the catheter. The two exhaust lumens also extend from shaft distal end to proximal end where they are exposed to the same cavity of the end cap. The coolant water runs axially inside the intake lumens from the distal to the proximal end then returns via the two exhaust lumens.

The previous investigation of the SAR heating pattern of the same microwave antenna by Xu *et al.* [25] proposed a simple one-dimensional (1-D) EM field, which is approximated by that of an infinitely long uniform line source. It results in a cylindrical EM field which has volumetric heat strength $q''' = A_t(2\alpha r + 1)e^{-2\alpha r}/r^3$. α is a known attenuation constant for uniform plane wave in a given media, A_t is a constant proportional to the microwave power which can be determined by curve fitting the predicted temperatures to those experimentally measured in the phantom gel. r is the radial distance from the center of the line source. However, as shown in Fig. 1, the microwave antenna is located with an offset s from the geometrical center so that the microwave field cannot

be treated as uniform in the angular direction. The catheter is designed this way to produce an asymmetric microwave field resulting in a preferential heating pattern. During the transurethral thermotherapy, the catheter can produce a greater microwave emission concentration in the anterior direction than that in the posterior direction, which prevents overheating the rectum. By considering this asymmetric configuration, Yuan *et al.* [26] extended the 1-D model to two dimensions to include its dependence on radial and angular direction by replacing the radial distance r by $r - s\cos\theta$ in the expression for the EM field power flux. However, none of these theoretical and experimental analyses considers the nonuniformity in the axial direction. In the preliminary analyses by Zhu *et al.* [27], the authors experimentally measured the three-dimensional (3-D) SAR distribution in the phantom gel by initial transient temperature gradients at various radial, angular, and axial locations in a microwave-equivalent phantom gel. A 3-D SAR expression was obtained by curve fitting. However, as mentioned above, since the SAR decayed rapidly in the radial direction due to the superficial penetration of microwave energy, its expression was fitted from the measurements in the near field ($r < 8$ mm). At the locations far from the center of the antenna, error percentages in temperature measurements increased due to low initial temperature elevations, which in turn resulted in the uncertainty of the SAR values. In addition, the fact that the SAR measurements scattered in the axial direction suggested that other fitting functions needed to be sought for the SAR expression. Thus, considering that the major concern in hyperthermia treatment for BPH was the temperature distribution within the prostate ($r < 20$ mm), more rigorous experiments were necessary to include a much wider region to obtain a more accurate and detailed 3-D microwave heating pattern of the T3 catheter.

In this study, a 3-D SAR expression was assumed based on the previous investigations. Then, a theoretical heat transfer model was developed to study the steady-state temperature profiles in the phantom gel by introducing this proposed SAR expression. The unknown parameters in this expression and a lumped value of the convection coefficient h due to the chilled water running around the antenna were determined using a least-square residual fit of the theoretical temperature predictions to the experimentally measured temperatures within the phantom gel. Both the SAR expression and h can be used in the future to theoretically model the temperature field in the prostate during transurethral thermotherapy.

II. Experiments

The experimental setup was similar to that described in Xu *et al.* [25]. A tissue-equivalent phantom was used to simulate smooth muscle tissue at 915 MHz. This gel mimics the electrical characteristics (dielectric constant and dissipation factor) of the tissue without vasculature. The reflection coefficient of the T3 microwave antenna was measured in the gel and it was in close agreement with that measured in the canine prostate.

The phantom gel was prepared according to the method from [12] and a formula provided by Urologix Inc. (Minneapolis, MN). Unlike the previous recipe provided in [1] with high water content (83%), the present gel had a water content of approximately 45%. Thus, the thermal conductivity k of the gel was expected to be quite different from that of water (0.59 W/m/K) or that of the previous recipe (0.56 W/m/K) [25]. In [21], thermal conductivities of aqueous solutions of ethylene glycol of various concentrations at room temperature was experimentally examined and fitted by an empirical equation. Using this empirical equation, $k = 0.38$ W/m/K was estimated for the gel based on the concentration of its major component, ethylene glycol. A more accurate measurement of k was taken in our lab using the thermal pulse-decay technique [8], and k was found to be equal to 0.396 W/m/K, which was used in this study to accurately calculate the SAR based on the steady-state temperature distribution in the phantom gel.

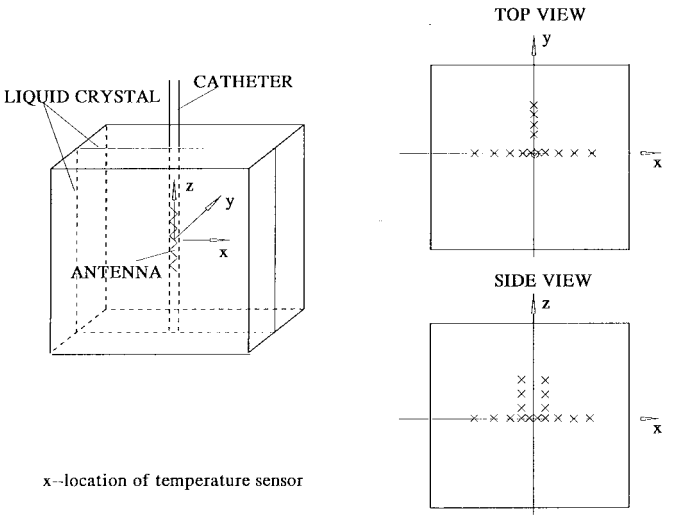

Fig. 2. Temperature sensor and catheter locations in the phantom gel.

The phantom gel was placed in a $14.4 \times 14.4 \times 14.4$ cm^3 cubic container. The Biot number can be roughly estimated as $hL/k \sim (25\ \text{W/m}^2\text{/K}) \times (0.072\ \text{m})/(0.4\ \text{W/m/K}) \sim 4.5$, which shows that the external convective thermal resistance is much smaller than the conductive thermal resistance inside the container. Considering the size of the catheter was approximately 3 mm in radius enclosing a 2.8-cm-long microwave antenna, the effects of the containers outside boundary are negligible. During each experiment, the T3 catheter was placed in the center of the gel (Fig. 2) and temperatures at different locations in the gel were measured by Fiber Optic Luxtron® temperature probes. The interaction of the temperature probes with the EM field was examined in the present study and previous investigations [14] by checking the temperature discontinuities when the microwave power was interrupted. The temperature discontinuity was found to be less than 0.1 °C, which indicated nonsignificant interaction. The distortion of the thermal field due to introducing the temperature probes was also negligible due to the small size of the temperature sensor (∼0.3 mm in diameter).

To minimize the number of temperature measurements, symmetry of the temperature distribution was first examined. If the steady-state temperature distribution in the homogeneous phantom is symmetric, then the power deposition is also symmetric about the same axis. The cross-sectional plane of the

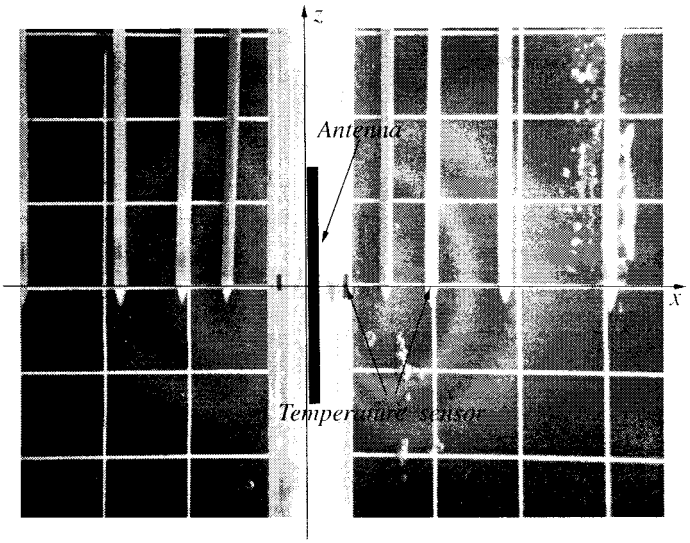

Fig. 3. Thermographic picture of the steady-state temperature field induced by 15 W heating in the x–z plane at $y = 0$ within phantom gel.

microwave antenna (Fig. 1) reveals the geometric symmetry about the x axis and possible symmetry about the x–y plane at the half length of the antenna ($z = 0$). In this experiment, symmetry of the temperature or SAR distribution about the x–y plane was determined by a liquid crystal thermometry which was installed in the x–z plane ($y = 0$) containing the catheter before the experiments. The liquid crystal sheet is black for temperatures <30 °C, and changes its color in four cycles over the range from 30 °C to 50 °C. Each cycle is, therefore, approximately 5 °C. Insertion of the sheet may introduce some thermal resistance and absorption. Since the sheet was flat and inserted in the plane where the temperature gradient perpendicular to the sheet is zero, the temperature field distortion was expected to be minor. The isotherms shown in Fig. 3, which was the steady-state temperature profiles induced by 15 W heating, clearly indicated the symmetry about the x–y plane at $z = 0$.

In our experiments, 16 Fiber Optic Luxtron® temperature probes with single or multiple sensors were used and situated parallel to the catheter. Among them, fourteen single-sensor probes approximately 5–10 mm apart were used to measure temperatures at different radial distances with the angular positions where maximum ($\theta = 0°$), intermediate ($\theta = 90°$) and minimum ($\theta = 180°$) microwave heating occurs (Fig. 2). Two other probes each with four in-line sensors (10 mm apart) were used to measure the axial temperatures in the x–z plane. During each experiment, temperatures were sampled and recorded every 5 s by a computer.

A total of five T3 catheters were examined in our experiments. The flow rate of the chilled water was about 100 ml/min. Prior to the experiment, the flow rate was tested to confirm that the temperature difference at the inlet and the outlet was less than 0.2 °C. During the experiments, the chilled water temperature T_w was set and maintained at 8 °C. Previous investigations [25]–[27] show that the SAR value is linearly proportional to the microwave power Q. The temperature elevation induced by 5 W microwave heating can be as much as 10 °C, which is much larger than the temperature sensitivity of the optical fiber sensor (0.2 °C). Further, at the lower power level, the steady-state temperature field is expected to be established within shorter period than at the higher power level. Therefore, only one power level ($Q = 5$ W) was used in the experiments.

For each catheter, the T3 system was turned on first, then the coolant water started running and the microwave power was set to 5 W to induce the microwave heating in the gel. During each experiment, as soon as 5 W was applied, temperatures were measured at all sensor locations and recorded into a data file on computer. The steady-state temperature field was determined when the temperature changes were less than 0.2 °C within 5 min. The data acquisition procedure lasted about 35 min during which the steady-state temperature field has been established in the gel.

III. Theory

A. SAR Distribution

To assume a reasonable SAR expression, we first examine the EM fields produced by an infinitely long line source and an infinitely large plane source, respectively. The power intensity of an individual EM field can be proportional to B^2. B is the magnitude of the magnetic field which is related to the geometry of the source and the absorption in a lossy medium as given by

$$B(r) \propto \begin{cases} e^{-\alpha r}/r, & \text{line source} \\ e^{-\alpha r}, & \text{plane source} \end{cases} \tag{1}$$

where r is the radial distance from the center of the line source or the perpendicular distance from the plane source. α is an attenuation constant equal to 0.0413 (mm^{-1}) for phantom gel and tissue [25]. Applying energy conservation to the control volume of interest, the volumetric power absorbed by the medium (i.e., SAR) can be found in (2), shown at the bottom of the page. In general, the radial component of the SAR can, thus, be given in the form of

$$\text{SAR} \propto e^{-2\alpha r}/r^n. \tag{3}$$

When n is equal to three and zero, it is equivalent to a line and plane source, respectively.

Based on (2) and (3), and results from previous investigations [25]–[27] of the microwave heating pattern, a 3-D SAR

$$\text{SAR} \propto \begin{cases} -\dfrac{1}{r}\dfrac{d}{dr}\left[rB^2(r)\right] \propto -\dfrac{1}{r}\dfrac{d}{dr}\left(r\,\dfrac{e^{-2\alpha r}}{r^2}\right) \propto \dfrac{(2\alpha r+1)\,e^{-2\alpha r}}{r^3}, & \text{line source} \\ -\dfrac{d}{dr}\left[B^2(r)\right] \propto -\dfrac{d}{dr}\left(e^{-2\alpha r}\right) \propto (2\alpha)\,e^{-2\alpha r}, & \text{plane source} \end{cases} \tag{2}$$

distribution (q''') is assumed in the form

$$q'''(r,\theta,z)\ (\mathrm{W/mm^3}) = C_t Q \frac{[2\alpha(r-s\cos\theta)+(n-2)]e^{-2\alpha(r-s\cos\theta)}}{(r-s\cos\theta)^n} e^{-z^2/z_0^2} \tag{4}$$

where Q is the microwave power (W) and C_t is a scale constant. One notes that C_tQ is equivalent to A_t in the SAR expressions in Xu *et al.* [25] and Yuan *et al.* [26], and this assumption is based on the previous result that A_t is proportional to the microwave power. n is an exponential constant, which depends on the configuration of the microwave antenna. The angular dependence of the SAR distribution is caused by an offset s of the microwave antenna from the geometric center of the catheter. The value of s is equal to 0.3 mm [27]. In the axial direction, we intend to use a simple function to describe the end effects of the microwave antenna. Considering the geometrical symmetry in the axial direction (z) a Gaussian function is used to fit the SAR dependence on z. z_0 can be viewed as the critical axial decay length over which 67% of microwave energy is absorbed. In this expression, C_t, n, z_0 are unknown parameters and will be determined later.

B. Heat Transfer Model Formulation and Assumptions

A geometric presentation of the T3 catheter inside a phantom gel is shown in Fig. 4. Origin of the coordinate system is set at the center of the catheter. The T3 catheter is represented by the inner cylinder. Since our analyses focus on temperatures produced in the gel surrounding the catheter, the cooling effect from the running water inside the catheter is modeled by a lumped constant convection coefficient h [27]. In the previous experimental study by Zhu *et al.* [27], the empirical h was calculated at two catheter locations in the angular direction when the water temperature was increased continuously from 8 °C to 20 °C. The results showed the geometric eccentricity and the coolant water temperature had very little effect on this value. During the experiments, the flow rate of the coolant water was also fixed as 100 ml/min. Based on the above reasons, it is highly speculative to assume a constant convective coefficient.

The surrounding phantom gel is modeled as an infinitely long cylinder of 14.4 cm in diameter with constant temperature T_∞ at the surface. This assumption is based on the following reasons. The phantom container is large enough to neglect the shape effect of the outside boundary, since temperature measurements on the outer surface of the container revealed very small temperature deviations from the environment temperature during the experiments. In Section IV, the axial temperature profile will show that the microwave heating has little influence in the region of $|z| > 70$ mm. Thus, this approximation is closely satisfied.

If the rectangular container is approximated by an infinite long cylinder, then the mathematical formulation can be greatly simplified. The governing equation in the gel is the traditional steady-state heat conduction equation with a volumetric heating source generated by the microwave

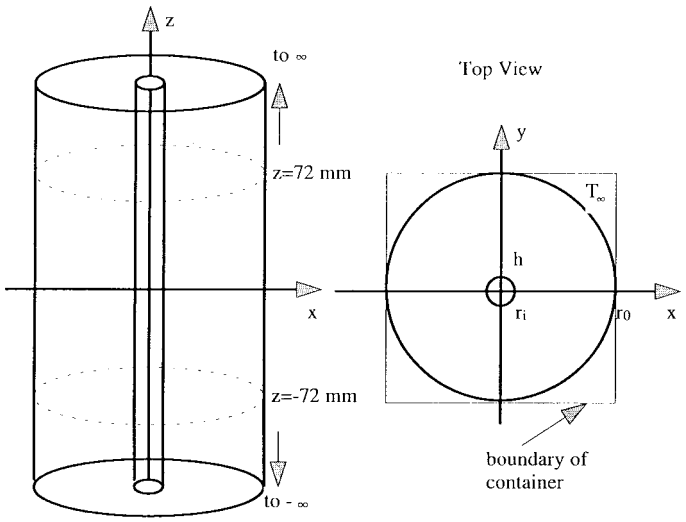

Fig. 4. The geometry of the phantom gel and the coordinate system in the mathematical modeling.

antenna, which is expressed by (4). Considering the symmetry in the system and in the SAR expression, the governing equation in the cylindrical coordinates and its corresponding boundary conditions, take the following form:

$$\frac{1}{r}\frac{\partial}{\partial r}\left(r\frac{\partial T}{\partial r}\right)+\frac{1}{r^2}\frac{\partial^2 T}{\partial\theta^2}+\frac{\partial^2 T}{\partial z^2}=-\frac{q'''(r,\theta,z)}{k}$$
$$r_0\ge r\ge r_i,\ \infty>z>-\infty$$
$$k\frac{\partial T}{\partial r}=h(T-T_w)\quad \text{at } r=r_i$$
$$T=T_\infty\qquad \text{at } r=r_0 \tag{5}$$

where k is the thermal conductivity of the phantom gel. The boundary conditions in the radial direction can be homogenized by introducing a function T', which satisfies Laplace equation and the boundary conditions

$$T'=T_\infty+(T_\infty-T_W)\frac{\ln(r/r_0)}{\ln(r_0/r_i)+k/(hr_i)}. \tag{6}$$

The temperature difference $\Delta = T - T'$ will satisfy the governing equation with homogeneous boundary conditions, which are given by

$$\frac{1}{r}\frac{\partial}{\partial r}\left(r\frac{\partial \Delta}{\partial r}\right)+\frac{1}{r^2}\frac{\partial^2 \Delta}{\partial\theta^2}+\frac{\partial^2 \Delta}{\partial z^2}=-\frac{q'''(r,\theta,z)}{k}$$
$$r_0\ge r\ge r_i,\ \infty>z>-\infty$$
$$k\frac{\partial \Delta}{\partial r}=h\Delta\qquad \text{at } r=r_i$$
$$\Delta=0\qquad \text{at } r=r_0. \tag{7}$$

Δ can be obtained by first solving a Green's function $W(r,\theta,z;\ \xi,\ \eta,\ \lambda)$, which satisfies Laplace's equation in the gel region except for the source point (ξ,η,λ) and all the boundary conditions. The boundary value problem for this singular solution is

$$\frac{1}{r}\frac{\partial}{\partial r}\left(r\frac{\partial W}{\partial r}\right)+\frac{1}{r^2}\frac{\partial^2 W}{\partial\theta^2}+\frac{\partial^2 W}{\partial z^2}$$
$$=\delta(r-\xi)\delta(\theta-\eta)\delta(z-\lambda)$$

$$k\frac{\partial W}{\partial r} = hW \qquad \text{at } r = r_i$$
$$W = 0 \qquad \text{at } r = r_0$$
$$W(r, -\theta+\eta, z) = W(r, \theta-\eta, z). \tag{8}$$

The solution to (8) is given by (A.14) in the Appendix

$$W(r, \theta, z{:}\,\xi, \eta, \lambda) = \sum_{m=0}^{\infty}\sum_{n=0}^{\infty} -\frac{f_{mn}(\xi)}{2\mu_n}[J_m(\mu_n r) + A_n N_m(\mu_n r)] \cdot \cos[m(\theta-\eta)]e^{-(z-\lambda)\mu_n}, \qquad z \geq \lambda$$
$$W(r, \theta, z{:}\,\xi, \eta, \lambda) = \sum_{m=0}^{\infty}\sum_{n=0}^{\infty} -\frac{f_{mn}(\xi)}{2\mu_n}[J_m(\mu_n r) + A_n N_m(\mu_n r)] \cdot \cos[m(\theta-\eta)]e^{+(z-\lambda)\mu_n}, \qquad z < \lambda \tag{9}$$

where A_n, μ_n, and $f_{mn}(\xi)$ are determined by (A.9a), (A.9b), and (A.11) of the Appendix. Finally, the solution of Δ can be easily constructed by

$$\Delta(r, \theta, z) = \int_{r_i}^{r_0}\int_{-\pi}^{\pi}\int_{-\infty}^{\infty} -\frac{q'''(\xi, \eta, \lambda)}{k} \cdot W(r, \theta, z{:}\,\xi, \eta, \lambda)\, d\xi\, d\eta\, d\lambda. \tag{10}$$

C. Least-Square Residual Fit

A least-square residual fit of the experimentally measured temperature difference $T - T'(\Delta)$ data to its analytical expression by (10) was performed to determine the unknown parameters C_t, n, z_0 in the SAR expression and the convection coefficient h. Those parameters were adjusted to minimize the square error of the temperature derivations at all temperature sensor locations. One fitting was obtained for all five catheters used in the experiments. Thus, the final result can be viewed as the average heating pattern induced by the T3 microwave antenna.

IV. Results and Discussions

Performing a least-square residual fit gives values of the four parameters in (4)

$$n = 2.2$$
$$C_t = 0.003\,16\,(\text{mm}^{-0.8})$$
$$z_0 = 18.5\,(\text{mm}^{-1})$$
$$h = 257\,(\text{W/m}^2/\text{K}). \tag{11}$$

The overall R value (coefficient of determination for the least-squares fitted curves) is 0.95.

Values of the convective coefficient h at the surface of the catheter was found to be 257 W/m^2/K. In the previous study [27], the convection coefficient h was roughly estimated based on the energy balance at two locations near the surface. Since the temperature gradient obtained at the surface was in fact an average value over a radial distance from $r = 3$ mm to $r = 8$ mm, its value was underestimated and, therefore, resulting in a lower h. The present fitting based on the detailed temperature profile is more accurate than the previous

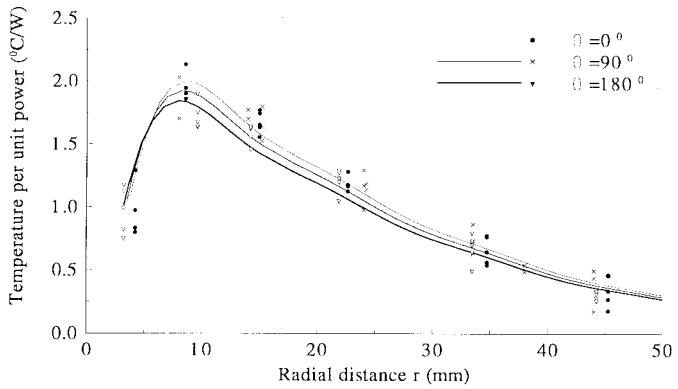

Fig. 5. Δ/Q predictions and measurements at different radial and angular locations within the gel.

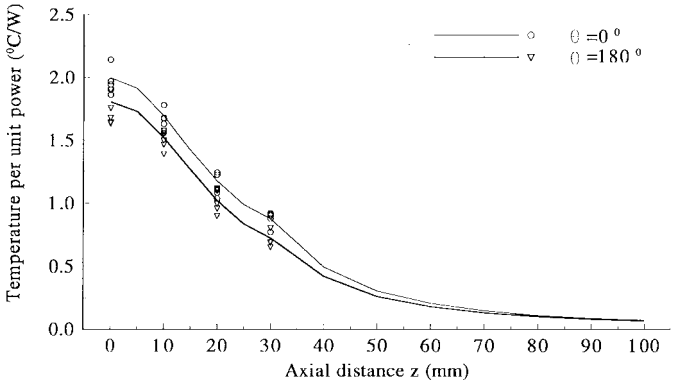

Fig. 6. Δ/Q predictions and measurements at different axial locations.

estimation. The convection coefficient h reflects the combined thermal resistance including the convective resistance between the water and the catheter inner surface, and the conductive resistance between the inner and outer silicon rubber wall of the catheter. If the first part of the thermal resistance is calculated using an h' of 600 W/m^2/K as estimated in Xu *et al.* [25], and the second part estimated by the thermal conductivity of silicon rubber and its thickness, then one can obtain that the lumped value of the convective coefficient to be approximately 270 W/m^2/K, which is in close agreement with the $h = 257$ W/m^2/K obtained in this study.

Figs. 5 and 6 present measured (symbols) and corresponding predicted (lines) Δ/Q at different radial, angular, and axial locations within the gel for all five catheters. It is noted that the microwave heating pattern for any of the five catheters does not deviate too much from each other. Fig. 5 shows that predictions in the radial direction agree well with the measured temperatures. The small scattering is primarily due to differences among catheters.

Fig. 6 clearly illustrates the nonuniformity of the temperature or SAR distribution in the axial direction. The newly used Gaussian function in the axial direction produces a very good temperature fit. The axial dependence of the SAR is important for theoretical modeling of thermal therapy since normal human prostate is a pear shape and approximately 30 mm in length. Clearly, the SAR cannot be treated as a constant in the axial direction. One can also find that temperatures approach

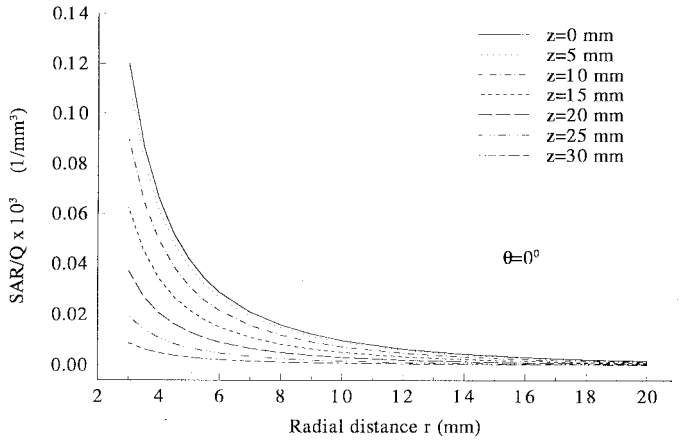

Fig. 7. Analytical SAR distributions in the radial direction at different axial locations.

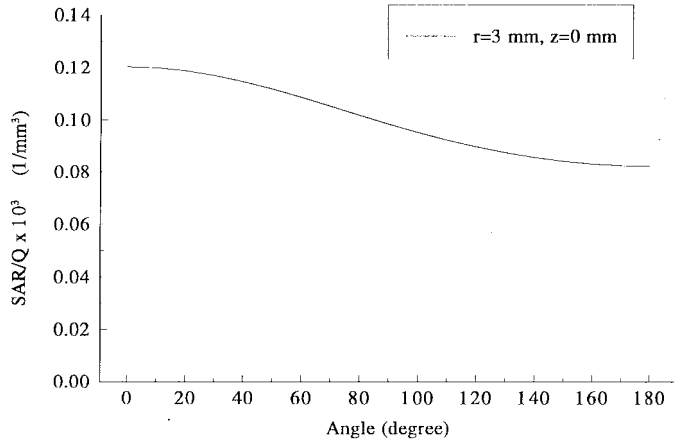

Fig. 8. Analytical SAR distribution in the angular direction.

zero when $z > 70$ mm, as shown in Fig. 6. This confirms that the effect of the microwave antenna on the top and the bottom boundary ($z = \pm 72$ mm) can be neglected and the infinitely long cylinder assumption is reasonable.

The SAR distributions calculated from (4) in the radial and axial direction were given in Fig. 7. Approximately 99% of the heat induced by the microwave antenna is absorbed in the near field ($r < 10$ mm). It is noted that the critical axial decay length $z_0 = 18.5$ mm is a little longer than the half length of the microwave antenna ($z = 14$ mm). About 67% and 98% of microwave energy is absorbed within $|z| < z_0$, and $|z| < 2z_0$ based on this Gaussian distribution. Fig. 8 illustrates the SAR variation in the angular direction. As expected, the offset of the microwave antenna from the geometric center of the catheter results in an approximately 30% less heat absorbed in the anterior than in the posterior direction.

In Fig. 9, the radial temperature distributions in the living tissue ($k = 0.5$ W/m/K [17]) induced by different microwave power levels were given. The temperature was estimated from (5) in which the SAR distribution was given by (4) and (11). Since the outside boundary in (5) is very large, the temperature field shown in Fig. 9 is expected to be similar to that within the prostate as if it is embedded in an infinite

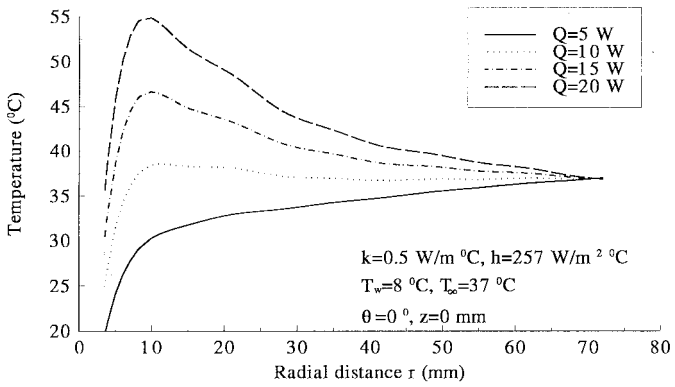

Fig. 9. Predictions of radial temperature distribution in tissue at different microwave power levels.

medium. These temperature profiles can be viewed as the upper limits of temperatures induced by different microwave heating levels because no blood perfusion was considered in this estimation. At lower microwave power level, such as 5 W, the contribution of the microwave radiative heating is small in comparison with that of the convective cooling at the catheter surface. Thus, there is no maximum observed in the radial temperature profile. At a higher power level, the microwave heating resulted in significant temperature elevations extending deep into the prostate region. As shown in Fig. 9, the location of the maximum temperature is approximately 10 mm from the center of the catheter and then 7 mm away from the catheter surface. In the *in vivo* temperature measurements in [13] and [14], peak intraprostate temperatures during the microwave treatment using the same kind T3 antenna were found about 5 mm from the catheter. This peak shift to the catheter surface may be due to the effect of the blood perfusion [17]. The minimum microwave power required to reach the treatment temperature 45 °C is found to be 15 W, while the prostatic urethral tissue is kept less than 42 °C. Obviously, the blood perfusion usually carries heat away from the prostate, therefore, higher microwave power level will be needed to achieve the same temperature (45 °C) especially when large increase in blood perfusion rate is expected during microwave heating [15].

To provide significant improvement in uro-dynamic function and symptoms, it is essential to find the optimal thermal dose needed in the prostatic thermal therapy. Undoubtedly, the heating pattern induced by the microwave antenna plays a critical role in temperature rise in the desired prostatic region. There are a number of previous investigations of the SAR distributions for various microwave antennas [4]–[6], [9], [10], [17], [19], [24], [25]. Similar to the present results, most of the microwave heat was found to be absorbed in the near field ($r < 15$ mm). In [4], [5], and [24], the EM fields produced by coaxial dipole antennas of different arrangements were investigated and the two-dimensional (2-D) SAR distribution was measured by determining the initial rate of temperature rise immediately following a step increase in the applied power. To avoid the power balancing requirement to produce symmetric heating around the dipole antenna, a helical antenna with a coiled structure was designed in [6], where the 2-D

distribution of SAR was also measured in a similar way. The SAR measurements in [4]–[6] and [24] provided important information in improving the microwave antenna. For example, the measurements showed that the heating pattern outside the helix had better longitudinal homogeneity than the dipoles and avoided the hot spot associated with the dipole junction. For the future theoretical modeling, some of the investigations not only measured the SAR distribution but also provided its fitted expression based on the analysis of the microwave power induced temperature field [17], [25]–[27]. In [17], the SAR distribution was fitted by an exponential decay in the radial direction and a cosine function in the angular direction for a transrectal microwave antenna. Strong angular dependence is expected due to the asymmetric location of the antenna. The SAR distribution based on the Maxwell equation of the EM field were also derived numerically [10]. Another approach to determine the SAR distribution is from the desired temperature field. There are several previous reports of optimization of numerically calculated SAR distribution [9], [19]. In the investigation by Chowdhyry *et al.* [9], the optimized SAR distributions were simulated from one type of inhomogeneous body model. It is important to note that blood perfusion in the prostate can also play a role in changing the tissue temperature. Thus, the previous and the present analyses of the SAR distribution in conjunction with the experimentally measured local blood perfusion data will provide valuable information in designing hyperthermia applicators.

Overall, this experiment investigated the detailed 3-D microwave heating pattern of the T3 catheter made by Urologix, Inc., and revealed a strong dependence of SAR in the radial, angular, and axial directions. It provides an accurate and 3-D analytical expression of the SAR distribution and a convective coefficient value h, which can be used as an important input in heat transfer modeling to predict temperature distributions in the prostate during the transurethral microwave hyperthermia. It may also be possible to use this SAR distribution in designing an improved microwave applicator in future.

APPENDIX

In this Appendix, we shall derive the Green's function $W(r, \theta, z: \xi, \eta, \lambda)$ for a point source at $r = \xi$, $\theta = \eta$, $z = \lambda$ that is described by (8) in the text. The governing equation and boundary conditions for W are the following:

$$\begin{aligned}
&\frac{1}{r}\frac{\partial}{\partial r}\left(r\frac{\partial W}{\partial r}\right)+\frac{1}{r^2}\frac{\partial^2 W}{\partial \theta^2}+\frac{\partial^2 W}{\partial z^2}\\
&\quad=\delta(r-\xi)\delta(\theta-\eta)\delta(z-\lambda)\\
&k\frac{\partial W}{\partial r}=hW, \qquad \text{at } r=r_i\\
&W=0 \qquad \text{at } r=r_0\\
&W(r,-\theta+\eta,z)=W(r,\theta-\eta,z). \qquad \text{(A.1)}
\end{aligned}$$

We assume that $W(r, \theta, z: \xi, \eta, \lambda)$ can be written in the separable form

$$W(r,\theta,z:\xi,\eta,\lambda)=\sum_{m=0}^{\infty}\Theta_m(\theta)W_m(r,z:\xi,\lambda) \qquad \text{(A.2)}$$

where $\Theta_m(\theta)$ satisfies

$$\begin{aligned}
&\frac{d^2\Theta_m(\theta)}{d\theta^2}=-m^2\Theta_m(\theta), \qquad m=0,1,2,\cdots,\infty\\
&\Theta_m(-\theta+\eta)=\Theta_m(\theta-\eta). \qquad \text{(A.3)}
\end{aligned}$$

The eigenfunction $\Theta_m(\theta)$ is obtained as

$$\Theta_m(\theta)=\cos[m(\theta-\eta)], \qquad m=0,1,2,\cdots,\infty. \qquad \text{(A.4)}$$

Substituting (A.4) into (A.2), we obtain

$$\begin{aligned}
&\sum_{m=0}^{\infty}\left[\frac{1}{r}\frac{\partial}{\partial r}\left(r\frac{\partial W_m}{\partial r}\right)-\frac{m^2}{r^2}W_m+\frac{\partial^2 W}{\partial z^2}\right]\cos[m(\theta-\eta)]\\
&\quad=c\delta(\theta-\eta)\delta(z-\lambda). \qquad \text{(A.5)}
\end{aligned}$$

Multiplying both sides of (A.5) by $\Theta_m(\theta)=\cos[m(\theta-\eta)]$ and integrating from $-\pi \le \theta \le \pi$, we obtain

$$\begin{aligned}
&\frac{1}{r}\frac{\partial}{\partial r}\left(r\frac{\partial W_0}{\partial r}\right)+\frac{\partial^2 W_0}{\partial z^2}\\
&\quad=\frac{1}{2\pi}\delta(r-\xi)\delta(\theta-\eta)\delta(z-\lambda) \qquad m=0\\
&\frac{1}{r}\frac{\partial}{\partial r}\left(r\frac{\partial W_m}{\partial r}\right)-\frac{m^2}{r^2}W_m+\frac{\partial^2 W_m}{\partial z^2}\\
&\quad=\frac{1}{\pi}\delta(r-\xi)\delta(z-\lambda), \qquad m=1,2,3,\cdots,\infty. \qquad \text{(A.6)}
\end{aligned}$$

Similarly, we assume that W_m can be written in the separable form

$$W_m(r,z:\xi,\lambda)=\sum_{n=0}^{\infty}R_n(r)Z_n(z:\xi,\lambda) \qquad \text{(A.7)}$$

where $R_n(r)$ satisfies

$$\begin{aligned}
&\frac{1}{r}\frac{d}{dr}\left(r\frac{dR_n(r)}{dr}\right)-\frac{m^2}{r^2}R_n(r)=-\mu_n^2R_n(r)\\
&k\frac{dR_n(r)}{dr}=hR_n(r), \qquad \text{at } r=r_i\\
&R_n(r)=0, \qquad \text{at } r=r_0. \qquad \text{(A.8)}
\end{aligned}$$

Equation (A.8) is a Bessel's equation of order m. The eigenfunction $R_n(r)$ is obtained as

$$R_n(r)=J_m(\mu_n r)+A_nN_m(\mu_n r) \qquad \text{(A.9)}$$

where

$$A_n=J_m(\mu_n r_0)/N_m(\mu_n r_0) \qquad \text{(A.9a)}$$

$$k[J_m'(\mu_n r_i)+A_nN_m'(\mu_n r_i)]=h[J_m(\mu_n r_i)+A_nN_m(\mu_n r_i)]. \qquad \text{(A.9b)}$$

Here J_m and N_m are the Bessel function of the first kind and the second kind, respectively. The coefficient A_n and the eigenvalue μ_n are determined by (A.9a) and (A.9b).

Similarly, substituting (A.9) into (A.7), multiplying both sides of (A.6) by $rR_n(r)$ and integrating from $r_i \le r \le r_0$, we obtain

$$Z_n''(z)-\mu_n^2Z_n(z)=F_{mn}(\xi)\delta(z-\lambda), \qquad n=0,1,2,\cdots,\infty \qquad \text{(A.10)}$$

where $F_{mn}(\xi)$ is expressed by

$$F_{mn} = \frac{\xi[J_0(\mu_n\xi) + A_nN_0(\mu_n\xi)]}{2\pi} \Big/ \int_{r_i}^{r_0} r[J_0(\mu_n r) + A_nN_0(\mu_n r)]^2\, dr \qquad m = 0$$
$$F_{mn} = \frac{\xi[J_m(\mu_n\xi) + A_nN_m(\mu_n\xi)]}{\pi} \Big/ \int_{r_i}^{r_0} r[J_m(\mu_n r) + A_nN_m(\mu_n r)]^2\, dr, \qquad m = 1, 2, 3, \cdots, \infty. \tag{A.11}$$

Equation (A.10) can also be written as

$$Z_n''(z) - \mu_n^2 Z_n(z) = 0, \qquad \text{at } z \neq \lambda \quad n = 0, 1, 2, \cdots, \infty$$
$$Z_n(\lambda^+) = Z_n(\lambda^-), \qquad Z_n'(\lambda^+) - Z_n'(\lambda^-) = F_{mn}(\xi). \tag{A.12}$$

The solution of $Z_n(z)$ is

$$Z_n(z) = -\frac{f_{mn}(\xi)}{2\mu_n} e^{-(z-\lambda)\mu_n} \quad z \geq \lambda$$
$$Z_n(z) = -\frac{f_{mn}(\xi)}{2\mu_n} e^{+(z-\lambda)\mu_n} \quad z < \lambda. \qquad n = 0, 1, 2, \cdots, \infty \tag{A.13}$$

Substituting (A.4), (A.7), (A.9), and (A.13) into (A.2), we obtain the following expressions for the Green's function $W(r, \theta, z: \xi, \eta, \lambda)$, which are used in Section III-B:

$$W(r, \theta, z: \xi, \eta, \lambda) = \sum_{m=0}^{\infty}\sum_{n=0}^{\infty} -\frac{f_{mn}(\xi)}{2\mu_n}[J_m(\mu_n r) + A_nN_m(\mu_n r)] \cdot \cos[m(\theta - \eta)]\, e^{-(z-\lambda)\mu_n}, \qquad z \geq \lambda$$
$$W(r, \theta, z: \xi, \eta, \lambda) = \sum_{m=0}^{\infty}\sum_{n=0}^{\infty} -\frac{f_{mn}(\xi)}{2\mu_n}[J_m(\mu_n r) + A_nN_m(\mu_n r)] \cdot \cos[m(\theta - \eta)]\, e^{+(z-\lambda)\mu_n}, \qquad z < \lambda \tag{A.14}$$

where A_n, μ_n, and $f_{mn}(\xi)$ are determined by (A.9a), (A.9b), and (A.11).

ACKNOWLEDGMENT

The authors wish to thank Urologix, Inc. for providing the transurethral thermal therapy system and the technical assistance during the experiments.

REFERENCES

[1] D. Andreuccetti, M. Bini, A. Ignesti, R. Olmi, N. Rubina, and R. Vanni, "Use of polyacrylamide as a tissue-equivalent material in the microwave range," *IEEE Trans. Biomed. Eng.*, vol. 35, pp. 275–277, 1988.

[2] L. Baert, F. Ameye, M. C. Pike, P. Willemen, M. A. Astrahan, and Z. Petrovich, "Transurethral hyperthermia for benign prostatic hyperplasia patients with retention," *J. Urol.*, vol. 147, pp. 1558–1561, 1992.

[3] L. Baert, F. Ameye, P. Willemen, J. Vandenhove, J. Lauweryns, M. A. Astrahan, and Z. Petrovich, "Transurethral microwave hyperthermia for benign prostatic hyperplasia: Preliminary clinical and pathological results," *J. Urol.*, vol. 144, pp. 1383–1387, 1990.

[4] M. A. Astrahan, M. D. Sapozink, G. Luxton, T. D. Kampp, and Z. Petrovich, "A technique for combining microwave hyperthermia with intraluminal brachytherapy of the oesophagus," *Int. J. Hyperthermia* vol. 5, pp. 37–51, 1989.

[5] M. A. Astrahan, M. D. Sapozink, D. Cohen, G. Luxton, T. D. Kampp, S. Boyd, and Z. Petrovich, "Microwave applicator for transurethral hyperthermia of benign prostatic hyperplasia," *Int. J. Hyperthermia*, vol. 5, pp. 283–296, 1989.

[6] M. A. Astrahan, K. Imanaka, G. Jozsef, F. Ameyes, L. Baert, M. D. Sapozink, S. Boyd, and Z. Petrovich, "Heating characteristics of a helical microwave applicator for transurethral hyperthermia of benign prostatic hyperplasia," *Int. J. Hyperthermia*, vol. 7, pp. 141–155, 1991.

[7] A. S. Bdesha, C. J. Bunce, J. P. Kelleher, M. E. Shell, J. Vukusic, and R. O'N Witherow, "Transurethral microwave treatment for benign prostatic hypertrophy: A randomized controlled clinical trial," *BMJ*, vol. 306, pp. 1293–1296, 1993.

[8] M. M. Chen and K. R. Holmes, "Thermal pulse-decay method for simultaneous measurements of thermal conductivity and local blood perfusion rate of living tissues," *Adv. Bioeng.*, pp. 113–115, 1980.

[9] D. Q. Chowdhury and S. C. Hill, "Numerical optimization of 3-D SAR distributions in cylindrical models for electromagnetic hyperthermia," *IEEE Trans. Biomed. Eng.*, vol. 38, pp. 1246–1255, 1991.

[10] G. B. Gentili, F. Gori, and M. Leoncini, "Electromagnetic and thermal models of a water-cooled dipole radiating in a biological tissue," *IEEE Trans. Biomed. Eng.*, vol. 38, pp. 98–103, 1991.

[11] Y. Homma and Y. Aso, "Transurethral microwave thermotherapy for benign prostatic hyperplasia: A 2-year follow-up study," *J. Endourol.*, vol. 7, pp. 261–265, 1993.

[12] "Tissue-simulating gel for medical research: The nonhardening, translucent gel more nearly simulates soft human or animal tissue," Langley Research Center, Hampton, VA, NASA Tech. Briefs, p. 80, Jan. 1992.

[13] T. R. Larson, D. G. Bostwick, and A. Corica, "Temperature-correlated histopathologic changes following microwave thermoablation of obstructive tissue in patients with benign prostatic hyperplasia," *Urol.*, vol. 47, pp. 463–469, 1996.

[14] T. R. Larson and J. M. Collins, "An accurate technique for detailed prostatic interstitial temperature-mapping in patients receiving microwave thermal treatment," *J. Endourol.*, vol. 9, pp. 339–347, 1995.

[15] ——, "Increased prostatic blood flow in response to microwave thermal treatment: Preliminary findings in two patients with benign prostatic hyperplasia," *Urol.*, vol. 46, pp. 584–590, 1995.

[16] V. T. Marteinsson and J. Due, "Transurethral microwave thermotherapy for uncomplicated benign prostatic hyperplasia," *Scand. J. Urol.*, vol. 28, pp. 83–89, 1994.

[17] G. T. Martin, M. G. Haddad, E. G. Cravalho, and H. F. Bowman, "Thermal model for the local microwave hyperthermia treatment of benign prostatic hyperplasia," *IEEE Trans. Biomed. Eng.*, vol. 39, pp. 836–844, 1992.

[18] F. Montorsi, G. Guazzoni, F. Berganaschi, P. Consonni, L. Galli, and P. Rigatti, "A comparison of transrectal hyperthermia, transurethral thermotherapy, urolume wallstent, and prostatic spiral for benign prostatic hyperplasia patients at poor operative risk," *Prostate*, vol. 24, pp. 156–161, 1994.

[19] N. Morita, T. Hamasaki, and N. Kumagi, "An optimal method in multi-applicator systems for forming a hot zone inside the human body," *IEEE Trans. Microwave Theory Tech.*, vol. 34, pp. 589–596, 1986.

[20] I. Nissenkorn and A. Meshorer, "Temperature measurements and histology of the canine prostate during transurethral hyperthermia," *J. Urol.*, vol. 149, pp. 1613–1616, 1993.

[21] Y. L. Rastorguev and Y. A. Ganiev, "Thermal conductivity of aqueous solutions of organic liquids," *Russian J. Physical Chem.*, vol. 40, vol. 7, pp. 869–871, 1996.

[22] J. J. M. C. H. de la Rosette, F. M. J. A. Froeling, and F. M. J. Debruyne, "Clinical results with microwave thermotherapy of benign prostatic hyperplasia," *Eur. Urol.*, vol. 23, suppl. 1, pp. 68–71, 1993.

[23] M. D. Sapozink, S. D. Boyd, M. A. Astrahan, G. Jozaef, and Z. Petrovich, "Transurethral hyperthermia for benign prostatic hyperplasia: Preliminary clinical results," *J. Urol.*, vol. 143, pp. 944–950, 1990.

[24] T. Z. Wong, E. Jonsson, P. J. Hoopes, B. S. Trembly, J. A. Heaney, E. B. Douple, and C. T. Coughlin, "A coaxial microwave applicator for transurethral hyperthermia of the prostate," *Prostate*, vol. 22, pp. 125–138, 1993.

[25] L. X. Xu, E. Rudie, and K. R. Holmes, "Transurethral thermal therapy (T3) for the treatment of benign prostatic hyperplasia (BPH) in the canine: Analysis using Pennes bioheat transfer," *Adv. Biol. Heat, Mass Transfer in Biotechnol.*, vol. HTD-268, pp. 31–35, 1993.

[26] D. Y. Yuan, J. W. Valvano, E. N. Rudie, and L. X. Xu, "2-D finite difference modeling of microwave heating in the prostate," *Adv. Biol. Heat, Mass Transfer in Biotechnol.*, vol. HTD-322, pp. 107–115, 1995.

[27] L. Zhu, L. X. Xu, D. Y. Yuan, and E. N. Rudie, "Electromagnetic (EM) quantification of microwave antenna for the transurethral prostatic thermotherapy," *Adv. Biol. Heat, Mass Transfer in Biotechnol.*, ASME, vol. HTD-337/BED-34, pp. 17–20, 1996.

Liang Zhu received the B.S. degree from the University of Science and Technology of China, Anhui, China, in 1988, and the Ph.D. degree from City University of New York, New York, in 1995.

She joined the faculty of the Department of Mechanical Engineering at University of Maryland Baltimore County, Baltimore, in January 1998, where she is an Assistant Professor. Her research interest is in the effects of vascular geometry and local blood perfusion on heat transfer in muscle tissues.

Lisa X. Xu received the Doctorate degree in engineering from the University of Illinois at Urbana-Champaign in 1991.

She worked as an Assistant Professor and Associate Professor in engineering science at the College of Staten Island of the City University of New York, Staten Island, for six years. She is currently an Associate Professor in the School of Mechanical Engineering at Purdue University, West Lafayette, IN. Her research is focused on the fundamental heat transfer mechanism in biological systems and its clinical applications.

Norbert Chencinski received the Doctorate degree in physics from the City University of New York.

He is a Professor of Physics at the College of Staten Island of the City University of New York, Staten Island. His early work includes magnetic field properties of A15 superconductors. His current work investigates the interaction of radiation with matter. This work includes radiation interaction with tissue, strong field effects in four wave mixing as well as dephasing phenomena in Bose–Einstein condensates.